16th World Conference on Earthquake Engineering, 16WCEE 2017
Santiago Chile, January 9th to 13th 2017
Paper N° 4306
Registration Code: S-M1463157728

SEISMIC COLLAPSE ASSESSMENT OF LOW-DUCTILITY CONCENTRICALLY-BRACED FRAME SYSTEMS

J. Sizemore[1], L. Fahnestock[2], E. Hines[3], C. Bradley[4]

[1] Graduate Research Assistant, Department of Civil and Environmental Engineering, University of Illinois at Urbana-Champaign; sizemor2@illinois.edu
[2] Associate Professor, Department of Civil and Environmental Engineering, University of Illinois at Urbana-Champaign; fhnstck@illinois.edu
[3] Professor of Practice, Department of Civil and Environmental Engineering, Tufts University; Principal, LeMessurier Consultants; ehines@lemessurier.com
[4] Graduate Research Assistant, Department of Civil and Environmental Engineering, Tufts University; cbradley@lemessurier.com

Abstract

Low-ductility steel concentrically-braced frame (CBF) systems that do not have seismic detailing or capacity design requirements are used extensively in moderate seismic regions of the United States. Structural behavior following brittle limit states is heavily dependent on secondary strength and stiffness, called reserve capacity. Recent full-scale cyclic tests and numerical simulations of low-ductility CBFs demonstrated potential sequences of damage and characteristics of reserve capacity for various system configurations. In addition, full-scale angle component and connection tests and corresponding numerical simulations have established a rigorous framework for modeling angle connections, which are very common in braced and gravity frame connections. With these full-scale component, connection and frame tests as the basis, seismic performance assessment of low-ductility CBFs has been conducted. This study considers a set of archetype buildings that represents common cases for the eastern and central US. Nonlinear response history analysis for ground motions scaled across a range of intensities is used to evaluate collapse potential of existing designs and to study enhanced design procedures that improve seismic stability. Selected results from this study are discussed in the present paper.

Keywords: Earthquake-Resistant Design; Concentrically-Braced Frames; Moderate Seismic Regions; Nonlinear Analysis

1. Introduction

Steel concentrically-braced frames (CBFs) in moderate seismic regions (Seismic Design Categories B and C) of the United States, are commonly designed using the "R = 3" provision within the current American Society of Civil Engineers (ASCE) Standard 7-10: *Minimum Design Loads for Buildings and Other Structures* [1]. This seismic force resisting system (SFRS) allows for a reduction in design base shear by the response modification coefficient, R, of 3, and is popular within moderate seismic regions due to its exemption from seismic detailing and proportioning requirements [1]. Interestingly, this provision offers nearly the same level of seismic force reduction as the ordinary concentrically-braced frame (OCBF), which permits designers to use R = 3.25 if the frame is seismically detailed in accordance with the requirements of the American Institute of Steel Construction (AISC) *Seismic Provisions for Structural Steel Buildings* [2]. Seismic detailing for OCBFs includes the necessity to consider amplified seismic demand in the design of select members and connections, and to adhere with local (b/t) and global (KL/r) slenderness limits for braces. Thus, when presented with the choice of designing a steel frame for a moderate seismic region, it is clear why a designer would prefer to use the R = 3 provision, as the ability to ignore the seismic detailing requirements outweighs the additional 8% (3.0 vs 3.25) of seismic force reduction obtained by selecting the OCBF system.

The ability for designers to use R = 3 for frames that are not specifically designed in consideration of inelastic deformation capacity is reliant on the inherent overstrength, ductility and reserve capacity in these frames. While it is possible for R = 3 frames to possess these favorable collapse prevention characteristics, the measure to which such characteristics are present can vary significantly from structure to structure and cannot therefore be considered as a reliable engineering design parameter. Reserve capacity is defined here as additional lateral force resisting capacity that is activated after significant damage to the primary SFRS, and is believed to have played a major role in collapse prevention of steel-framed buildings during the 1994 Northridge [3, 4], 1995 Hyogo-ken Nanbu [5] and 2010/2011 Christchurch [6] earthquake events. Unlike frames in high seismic regions, whose post-

elastic behavior is best characterized as highly ductile, frames in low and moderate seismic regions have a low-ductility post-elastic behavior comprising brittle limit states such as the fracture of a brace or a connection. Thus, the collapse prevention performance of these frames is largely dependent on reserve capacity [7, 8].

Several sources of reserve capacity have been studied to date, with a predominant focus on connection behavior. Connection behavior within steel-framed buildings encompasses both simple and partially-restrained beam-column connections that are part of gravity framing [3, 9, 10, 11, 12, 13, 14, 15], and on braced frame beam-column-gusset connections [16, 17, 18]. Another prominent source of reserve capacity is the frame action (beam and column bending) which results following a loss of one or more braces within a braced frame due to low-cycle fatigue fracture from significant local buckling or from brace-gusset weld fracture. Some sources of reserve capacity are dependent on the type of mechanism that forms. For example, beam bending at midspan following asymmetrical damage to braces within chevron CBFs can provide large amounts of reserve capacity [19, 20]. In some cases, a specific sequence and type of damage must occur before a particular source of reserve capacity can be activated. For example, if a brace-gusset weld fractures cleanly in a slotted HSS connection, the brace slot may re-engage onto the gusset place in compression to provide reserve strength and stiffness through bearing [8, 20, 21]. Understanding the sources of reserve capacity that contribute to collapse prevention is a key step towards a goal of harnessing and enhancing reserve capacity such that it can be coherently and reliably used in design.

2. Experimental Testing Program

Many of the recent design studies and numerical simulations performed by the authors and cited above were initiated from a project funded by the US National Science Foundation titled *Reserve Capacity in New and Existing Low-Ductility Braced Frames*. The project's goal is to understand the influence of reserve capacity on the seismic performance of low-ductility steel CBFs up to the point of collapse. One component of the project is experimental testing. To date, testing has been performed on angle components, beam-column connections, and entire frames.

2.1 Angle component and beam-column connection tests

Previous experimental studies have shown that beam-column connections within gravity bays and beam-column-gusset connections within braced bays may provide significant amounts of reserve capacity. Experimental studies thus far have shown that geometric properties such as angle thickness, bolt gage, and bolt dimension have the largest influence on the strength and stiffness of angles [22, 23]. In a comprehensive study of 140 angle tests [15] these geometric properties and others were varied parametrically in both monotonic and cyclic tests to determine the behavior of a large range of angle sizes commonly used in construction. This study was followed by a test program of 24 beam-column connections both with and without top- and seat-angles, which is currently underway.

2.2 Frame tests

Two full-scale CBF experiments were conducted to study limit state progression and post-elastic behavior of low-ductility CBFs. Test units were constructed using SFRS designs of a three-story prototype building for Boston, MA according to forces specified in ASCE 7-05 [24]. The two test units were: (1) an $R = 3$ frame with braces in the chevron configuration; and (2) an OCBF with braces in the split-x configuration. These tests illustrate the influence that a designer's choice of system type ($R = 3$ or OCBF) and system configuration (chevron or split-x) can have on post-elastic behavior and reserve capacity. For example, without *b/t* limits on braces within an $R = 3$ frame, braces are more susceptible to local buckling and low-cycle fatigue related fracture than their OCBF-brace counterparts. Additionally, the requirement of designing brace-gusset welds in OCBFs for amplified seismic demands increases the potential for post-elastic frame ductility prior to a brittle limit state resulting from brace-gusset weld fracture. A thorough summary of the behavior of these frames may be found in separate papers by the authors [19, 20].

3. Numerical Model Development

From the component level (angle tests), to the connection level (beam-column tests), to the structural level (frame tests), the experimental test programs provided invaluable insights into structural behavior of low-ductility CBFs.

The test data additionally provided an important benchmark for creating and validating numerical models so that further exploration of reserve capacity and collapse prevention of low-ductility CBFs could continue. Numerical frame models were developed using the *OpenSees* simulation platform [25]. The *Steel02* material type and fiber-based cross-sections were used for all beams, column, and braces. Cyclic degradation was approximated in braces using the *Fatigue* material, with inputs calculated from an empirical equation for low-cycle fatigue in HSS braces [26]. To facilitate brace buckling, eight elements were used for each brace in conjunction with an initial out-of-straightness of $L/1000$.

Beam-column and beam-column-gusset connections within the gravity bays and braced frame bays, respectively, were modeled using a fiber-based section with fibers at each bolt line. The primary component in this model is hysteretic angle behavior, but angle bearing and bolt slip are also considered. Hysteretic angle behavior is determined using a component-based angle model developed by the authors and validated by the comprehensive angle test suite [15]. The beam-column connection model was validated by comparison with the results of a separate connection test program on bolted-bolted and bolted-welded beam-column connections [11], and will be further confirmed with future beam-column connection tests. Brace-gusset connections are composed of a zero-length element, which contains both rotational and translational springs. The rotational springs use the *Hysteretic* material and facilitate brace buckling. The stiffness and strength inputs for this material are calculated for each gusset plate size and thickness using fundamental equations related to out-of-plane gusset bending [27]. The translational springs use an elastic material with a capacity limit to capture brace-gusset weld fracture. When the brace-gusset weld capacity is reached, the corresponding zero-length element is removed from the model, simulating a weld fracture. Due to the unpredictable nature of brace re-engagement in compression, this phenomenon was not considered in this study. In other words, once a brace-gusset weld fracture occurs, the interface can no longer transfer force in either tension or compression for the remainder of the simulation.

The schematic in Figure 1a displays each of these connection types within the frame in addition to the locations of the beam-column fiber elements and rigid elements. Note that rigid elements were used to consider the depth of column and beam sections as well as the stiffening effect from gusset plates. The global element discretization for the numerical model is shown in Figure 1b.

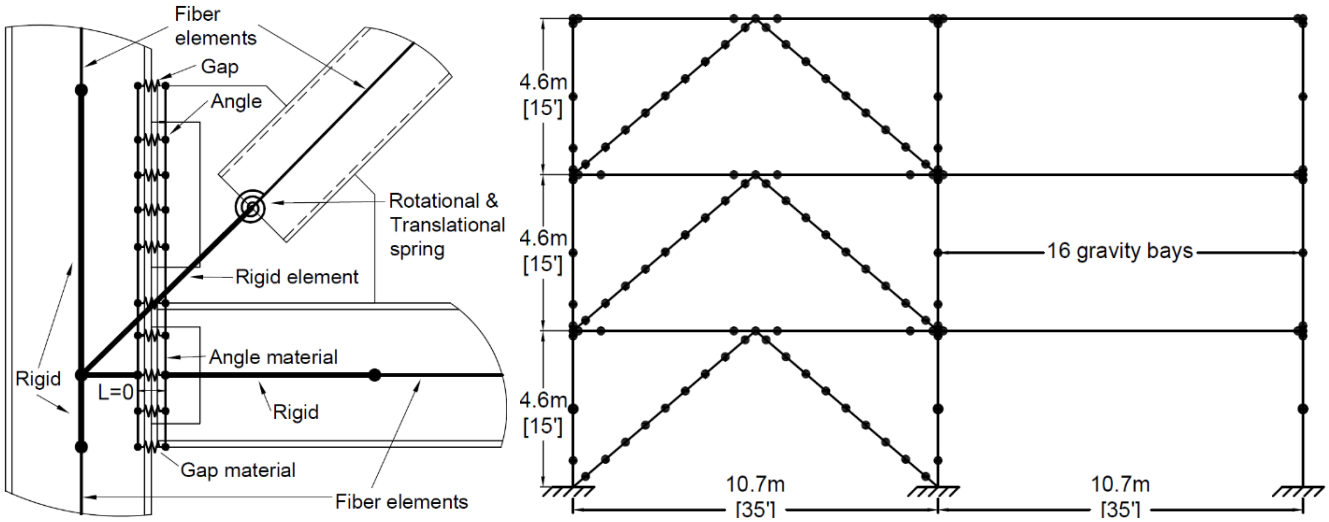

Figure 1 – Numerical model: (a) connection discretization and elements; (b) global frame discretization.

4. Numerical Simulations

Using the validated numerical model, additional prototype frames were designed and modeled to continue the investigation started with the full-scale frame tests on the influences that system type (R = 3 CBF or OCBF) and system configuration (chevron or split-x) have on reserve capacity and collapse prevention.

4.1 Static simulations

The first set of numerical simulations used a static-cyclic loading protocol with a lateral load profile defined using the equivalent lateral force procedure from ASCE 7. Similar to the companion full-scale tests [19, 20, 28], these simulations were performed on the braced frames only (no gravity bays), and for lateral loads only. Frames were cycled to incrementally larger roof drifts, δ_R/H, up to a maximum of ± 2%. The primary test matrix for this study consisted of eight braced frames that were developed by varying three parameters: (1) system type; (2) system configuration; and (3) whether the approximate period (T_a) or calculated period (T_c) was used to determine the design base shear in allowance with ASCE 7. Brace-gusset weld fracture was the governing limit state in the analyses of these eight frames, owing largely to the assumption of a nominal weld capacity, R_n, which resulted in the welds having a smaller capacity than the brace buckling capacity for all frames other than the split-x OCBFs. This study revealed that the weld capacity played a dominant role in where initial damage occurred within the test frames, the type of mechanism that occurred, and the amount of reserve capacity observed. As a result, additional test frames were designed and simulated under assumptions of varying levels of weld overstrength up to a maximum of $1.8R_n$, in agreement with the amount of weld overstrength observed experimentally. In total, six distinct mechanisms were observed during these static cyclic simulations as shown in Figure 2.

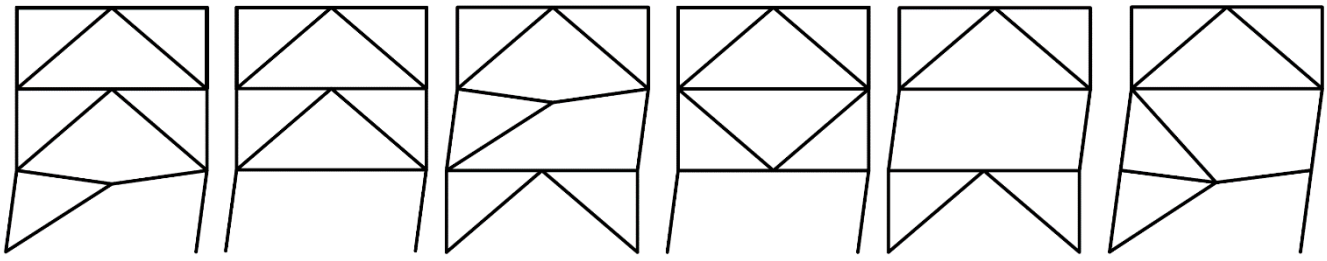

Figure 2 – Schematic deformed shapes for the six mechanisms observed in the static simulations: (a) chevron first-story single brace; (b) chevron first-story double brace; (c) chevron second-story single brace; (d) split-x first-story double brace; (d) split-x second-story double brace; (e) split-x two-story.

As the schematics in Figure 2 show, the selection of system configuration (chevron or split-x) was found to have a significant influence on the type of mechanism that forms. Most noticeably, the chevron configuration allows for the development of a mechanism driven by column bending and beam midspan bending following the loss of a brace (Figures 2a and 2c). This mechanism can persist as long as the connections have adequate strength and ductility, and the beam is not strong enough to transfer sufficient axial force to result in brace-gusset weld fracture in the remaining brace within a damaged story in a chevron configuration. If this brace-gusset weld fracture occurs, the bending mechanism is lost and the reserve capacity comes predominantly from column bending (Figure 2b). This occurred in static simulations of the OCBF chevron frames studied due to the criteria in the AISC *Seismic Provisions* that beams in these frames be capacity designed for a potential force imbalance between the compression and tension braces, increasing their size significantly.

The indeterminacy of the split-x configuration provided for a more direct alternate load path following the loss of a brace. As a result, a second brace was lost in the split-x frames when cycling back in the opposite direction following the loss of the first brace. In most cases, this resulted in a mechanism governed strictly by column bending (Figures 2d and 2e). When brace loss occurred in adjacent stories within a split-x frame, a two-story mechanism formed comprising both beam and column bending (Figure 2f). However, this mechanism provided poor reserve capacity as the significant drop in stiffness diminished any reserve capacity which beam bending could have provided. To show an example of how beneficial the beam bending mechanism displayed by the chevron frames is with respect to reserve capacity, base shear (V_B) vs roof drift (δ_R/H) plots are provided in Figure 3 for two identically designed R = 3 frames which differ only by their brace configuration. Frames were loaded cyclically using the equivalent lateral force design profile. Although both frames exhibited a second-story mechanism, the reserve capacity of the split-x frame (550kN) at δ_R/H = 1.0% is noticeably less than the reserve

capacity of the chevron frame (900kN) at the same drift level. This difference in reserve capacity (350kN) is attributable to bending of the W12x35 beam, which spans atop the second story in the chevron frame.

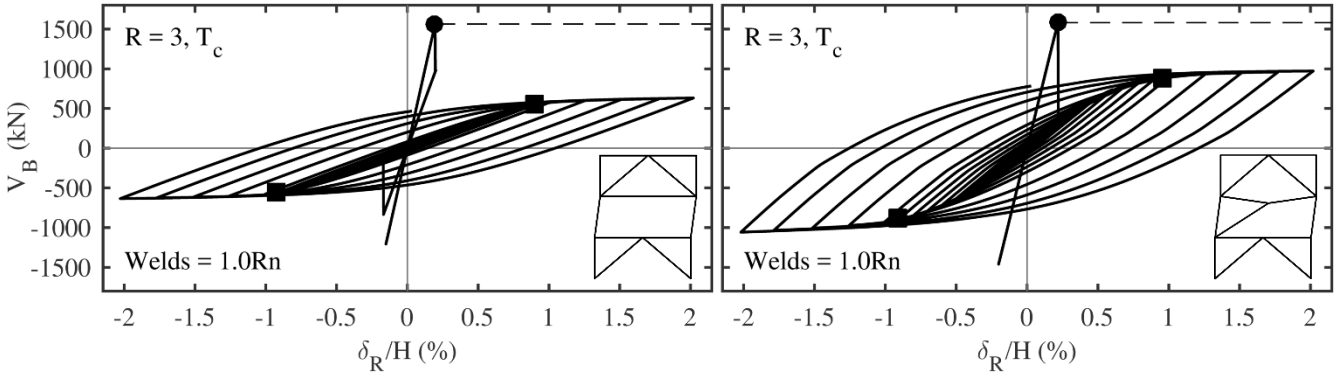

Figure 3 – Static cyclic response of two *R* = 3 frames designed for the same loads but with braces in different configurations: (a) split-x configuration; and (b) chevron configuration.

The selection of system type (*R* = 3 or OCBF) most significantly affected elastic capacity of the frames studied. The most common limit state was brace-gusset weld fracture, so when the brace-gusset welds in the OCBFs were designed for the amplified seismic demand as specified by the *Seismic Provisions*, the elastic capacity of these frames was increased substantially over the *R* = 3 counterpart. When the weld strength exceeded the buckling capacity, the influence of the *b/t* limits on braces within OCBFs was realized as these braces became less susceptible to low cycle fatigue related to local buckling. In general, the detailing requirements for OCBFs increased the size of members and connections, which in turn increased both elastic capacity as well as reserve capacity. A thorough summary of these static-cyclic numerical simulations is provided elsewhere [29].

4.2 Dynamic simulations

Based on the results from the full-scale tests and the static simulations, a new test matrix was proposed for dynamic analyses, with the goal of further identifying differences in structural behavior resulting from the distinction of system type and system configuration. Unlike the static cyclic simulations, this study includes the gravity bays and destabilizing effects of gravity loads. Three design parameters are varied in this test matrix: (1) system configuration (chevron or split-x); (2) system type (*R* = 3 or OCBF); and (3) number of stories (3, 6, or 9). Other variables such as bay width (10.7m [35ft]) and story height (4.6m [15ft]) were kept consistent with previous prototype designs. Dynamic simulations for four prototype buildings have been completed to date: (1) 3-story *R* = 3 chevron, (2) 3-story *R* = 3 split-x, (3) 3-story OCBF chevron, and (4) 3-story OCBF split-x. Member sizes and diagonal brace-to-gusset weld sizes for the four braced frames are summarized in Tables 1 and 2, respectively. Brace-gusset weld capacities were calculated assuming a 70ksi weld metal, with no resitance factors. Beam-column and gusset-column connections within the braced frames are composed of 2L4x4x1/2 with 3 rows of 25.4mm [1”] diameter A490 bolts in all frames. Beam-column connections within the gravity bays are composed of 2L4x4x1/4 with 3 rows of 25.4mm [1”] diameter A490 bolts.

Table 1. Braced frame designs for dynamic simulations – member sizes

Frame Designation	Story 1 Braces (HSS)	Story 2 Braces (HSS)	Story 3 Braces (HSS)	Level 2 Beam	Level 3 Beam	Roof Beam	Columns
R = 3 chevron	9x9x1/4	8x8x1/4	6x6x1/4	W12x40	W12x40	W12x26	W12x53
R = 3 split-x	9x9x1/4	8x8x1/4	6x6x1/4	W12x26	W16x40	W12x26	W12x53
OCBF chevron	8x8x1/2	8x8x1/2	8x8x1/2	W30x90	W24x68	W14x22	W12x58
OCBF split-x	6x6x1/2	6x6x3/8	8x8x1/2	W12x26	W16x40	W14x22	W12x53

Table 2. Braced frame designs for dynamic simulations – brace-gusset fillet weld sizes and capacities

Frame Designation	Story 1	kN	Story 2	kN	Story 3	kN
R = 3 chevron & R = 3 split-x	l = (4) x 279mm d = 6.4mm	1470	l = (4) x 229mm d = 6.4mm	1200	l = (4) x 152mm d = 4.8mm	600
OCBF chevron & OCBF split-x	l = (4) x 330mm d = 6.4mm	1710	l = (4) x 254mm d = 6.4mm	1330	l = (4) x 203mm d = 4.8mm	800

The prototype buildings were subjected to a suite of 15 Site Class D MCE-level ground motions (GMs) for Boston, MA [7]. Response spectra for the GMs are plotted in Figure 4 along with the 2008 maximum considered earthquake (MCE) spectrum for Boston. The fundamental period of the prototype buildings that have been designed and simulated to date are also indicated. The OCBF chevron has a noticeably shorter fundamental period (0.601s) as a result of the significantly stockier HSS8x8x1/2 braces in this building, which are dictated by the combined *KL/r* and *b/t* limitations for OCBF chevrons.

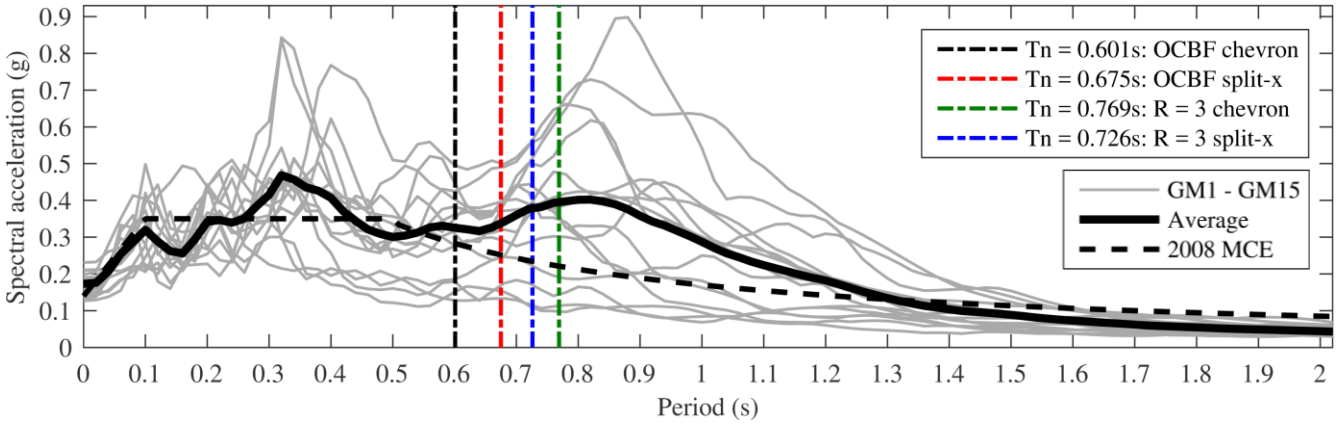

Figure 4 – Suite of 15 Boston ground motions used for incremental dynamic analyses [7].

4.2.1 Single-record dynamic simulations

A direct comparison of the behavior of the four frames subjected to an MCE-level earthquake is provided in Figure 5, for GM 13. Deformed shapes are plotted for the four frames at the end of the GM. Although none of the four frames collapsed under this ground motion with a scale factor (*SF*) equal to 1.0, significant amounts of drifts were incurred in the R = 3 frames. The R = 3 split-x formed the two-story mechanism which was previously observed in the static numerical simulations and was found to have poor reserve strength (Figure 2f). The response of the R = 3 split-x clearly shows two modes of behavior: (1) a longer-period response associated with the two-story mechanism; and (2) a more localized short-period response associated with the upper-story beam bending mechanism. The R = 3 chevron displayed a similar bi-modal behavior, with a longer-period responses associated with the loss of a first story brace. Higher mode behavior occurred in many of the dynamic simulations, and allowed damage to spread more evenly across multiple stories in contrast to the static analyses where damage was often concentrated to a single story as a result of the constant lateral force profile. The OCBFs experienced large amounts of damage as well, but residual drifts in these frames were smaller than in their R = 3 counterparts. The larger beams within the OCBF chevron prevented significant drifts from occurring despite damage to every story.

Two single-record collapse cases (R = 3 chevron and R = 3 split-x) for GM 4 are shown in Figures 6 and 7, respectively. The R = 3 chevron collapsed under GM 4 with *SF* = 2.4, and the R = 3 split-x collapsed under GM 4 with *SF* = 1.0. The sequence of damage leading up to collapse is shown with associated base shear and deformed shapes as well as the evolving damaged structural period, T_n, following each limit state. For the R = 3 chevron, limit state progression began with a first-story brace-gusset weld fracture at t = 6.12s and a base shear, V_B, of

2150kN. Loss of a brace within the first story of this chevron frame increased T_n by nearly 200%, from 0.769s to 2.25s. This was followed quickly by a third-story brace-gusset weld fracture at t = 6.48s, and finally a second-story brace-gusset weld fracture at t = 28.10s. Loss of an upper story brace had no measurable effect on T_n or V_B.

For the R = 3 split-x, limit state progression began with a first-story brace-gusset weld fracture at t = 15.39s and a base shear, V_B, of 1950kN. Unlike the R = 3 chevron, however, this limit state increased T_n by only 45%, from 0.726s to 1.05s. This demonstrates robust load redistribution in the split-x configuration. A two-story mechanism occurs at t = 3.70s, which results in a large increase in T_n from 1.05s up to 3.70s. Later in the analysis at t = 37.08s, the remaining brace in the second story is lost from a brace-gusset weld fracture, which ultimately leads to collapse.

The single-record responses show a stark contrast from what was observed in the static analyses. The static analyses used a constant force profile, thus large drops in stiffness following damage to one story protected other stories from incurring damage. Under a dynamic analysis, the remaining stories were not as protected as Figures 6 and 7 show. This difference in behavior is attributable to higher mode behavior altering the force profiles throughout the analysis. All collapse cases observed were ultimately driven by global P-delta effects, which created a soft first-story following loss of a first-story brace. In other words, collapse was not observed during this study unless a first-story limit state occurred.

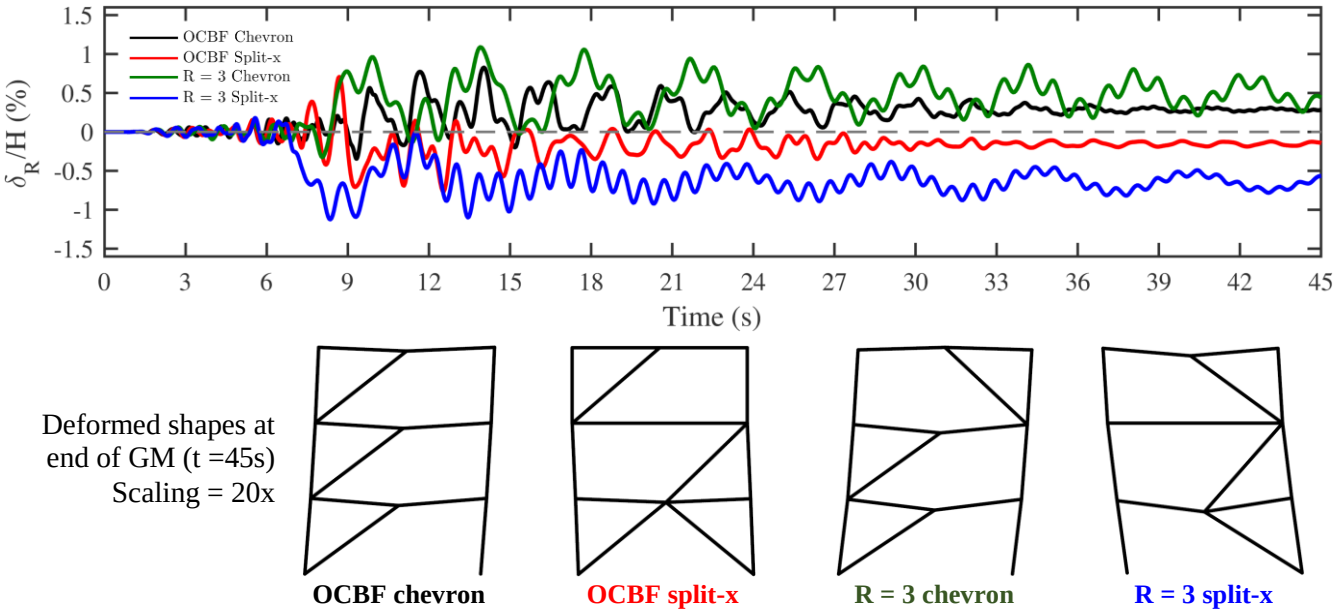

Figure 5 – Behavior for the four CBFs studied when subjected to GM 13 (*SF* = 1.0).

4.2.2 Multi-record dynamic simulations

Further simulations were performed by incrementally scaling the GMs using *SF* steps of 0.2, starting from *SF* = 0.2. Once building collapse was identified for a given GM, no further *SF*s were tested for that particular GM. Thus, the phenomenon of *structural resurrection* – which is when a building experiences collapse at some *SF*, only to reappear as non-collapsing at a higher *SF* – was not investigated [30]. As discovered during this investigation, the highly nonlinear behavior of these building models resulted in different damage sequences for the same ground motion with only slight changes in *SF*. Thus, there is a strong likelihood that the buildings might survive the GMs studied for some *SF*s beyond where the first failure was observed, and this is being investigated in ongoing work. Nevertheless, response up to the first *SF* at which collapse is observed still provides a viable benchmark for comparing the prototype buildings. The first *SF* corresponding to collapse for each of the four buildings studied and all 15 GMs studied is shown in Table 3. The multi-record incremental dynamic analyses (IDAs) are summarized in Figure 8 as a series of 16%, 50% (median), and 84% fractile curves for each prototype building [29]. The curves are created by recording the maximum observed story drift within a building at each *SF* across

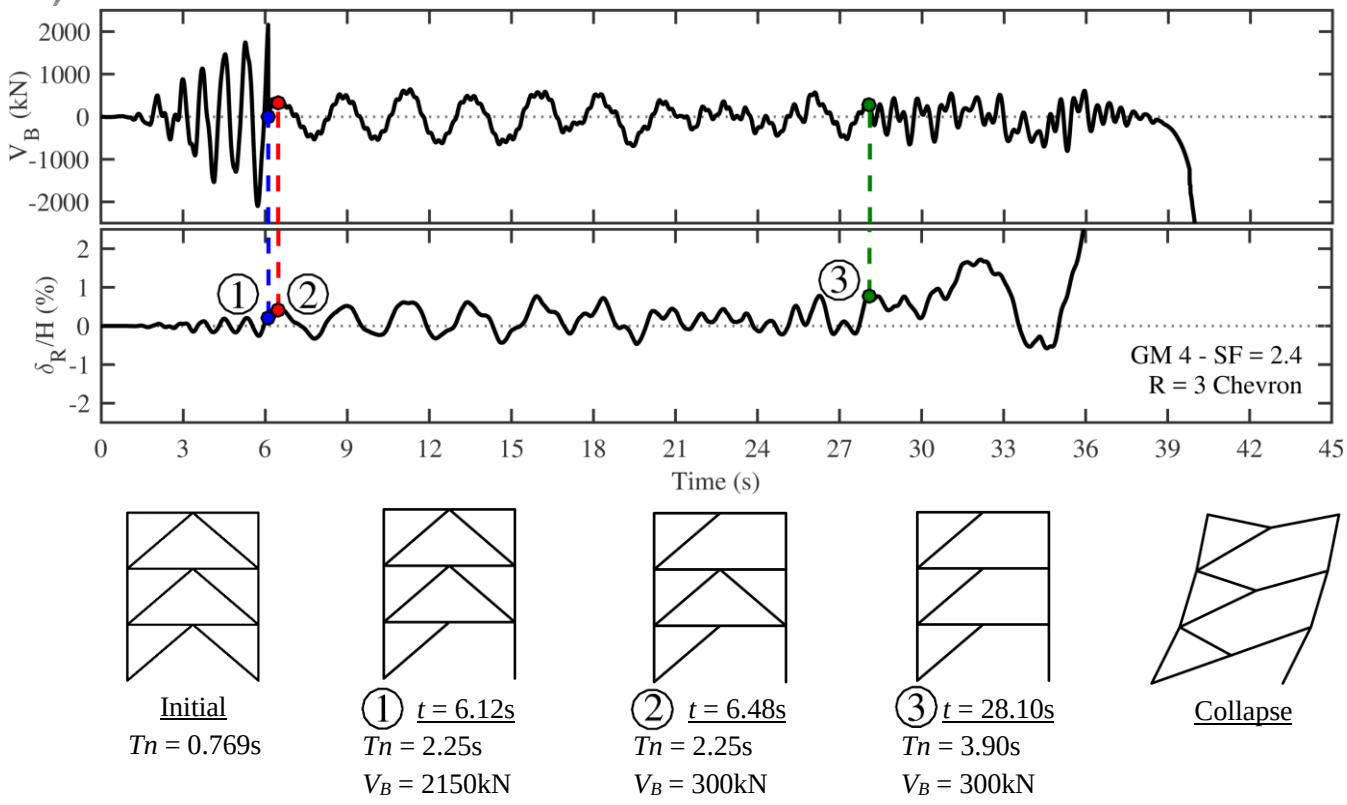

Figure 6 – Limit state progression leading up to collapse: R = 3 chevron frame, GM 4 with SF = 2.4.

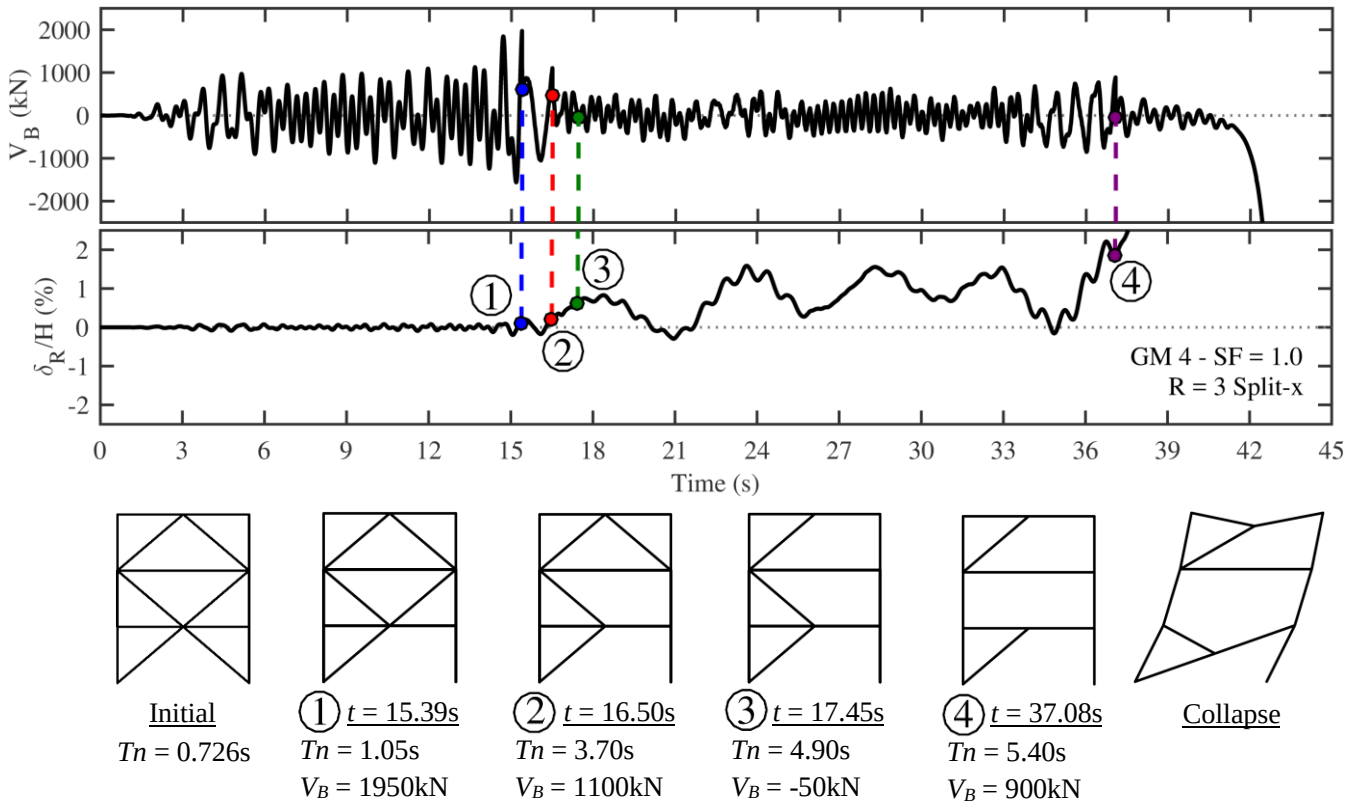

Figure 7 – Limit state progression leading up to collapse: R = 3 split-x frame, GM 4 with SF = 1.0.

all ground motions. Median, 16%, and 84% fractiles are calculated until collapse occurs in 50% (8/15), 84% (13/15), or 16% (3/15) of GMs, respectively, at which point the calculated values yield infinity.

Table 3 – Lowest scale factor (*SF*) corresponding to building collapse

Prototype Building	Ground Motion															Avg *SF*
	1	2	3	4	5	6	7	8	9	10	11	12	13	14	15	
R = 3 chevron	2.4	4.6	3.2	2.4	1.8	1.4	3.6	2.2	1.4	1.8	2.4	2.0	2.8	1.8	3.0	2.4
R = 3 split-x	1.6	1.8	1.2	***1.0***	1.2	***1.0***	2.4	1.6	***0.8***	1.8	1.4	1.4	1.8	1.4	2.2	1.5
OCBF chevron	6.4	8.0	5.0	4.8	2.8	2.2	6.6	6.2	3.2	4.0	4.2	5.4	5.2	2.6	10.2	5.1
OCBF split-x	2.0	4.4	2.0	2.6	1.6	***1.0***	5.2	1.6	2.0	2.0	1.6	1.4	1.4	1.2	3.8	2.2

For all CBFs studied, the dominant limit state was fracture of a brace-gusset welded connection. As indicated by the single-record studies, the *R* = 3 split-x building had the worst performance of the four buildings tested, failing under 3 (*SF* = 1.0 or less) GMs. Collapse at *SF* = 1.0 or less occurred in only one other frame, the OCBF split-x, and only for GM6. This result confirms observations that were made from the large scale split-x test as well as split-x static simulations. The split-x configuration allows for beneficial initial ductility, as the frame indeterminacy provides an alternate load path through the tension braces after buckling occurs within one or both stories of an "X". As a result, this ductility is largely reliant on the brace-gusset weld capacities within the frame. Unlike the OCBF seismic provisions, which require brace-gusset welds to be designed for two times the seismic effect, the *R* = 3 provisions by definition have no detailing or proportioning requirements for these connections. Thus, brace-gusset welds within an *R* = 3 CBF will generally have a lower capacity than welds within a similar OCBF. For the 3-story CBFs studied, the brace-gusset welds within the OCBFs had capacities 10%-33% higher than welds within their *R* = 3 CBF counterparts. As observed previously, the majority of reserve capacity from split-x CBFs comes from column bending after brace-gusset weld fracture. Because both split-x CBFs were composed of identical column sizes, the additional weld capacity is the primary reason the OCBF split-x displayed superior collapse prevention compared to the *R* = 3 split-x.

Similar to how the OCBF split-x outperformed the *R* = 3 split-x, the OCBF chevron outperformed the *R* = 3 chevron. Although the brace-gusset welds in the OCBF chevron were stronger than those in the *R* = 3 chevron, the superior performance of the OCBF chevron was related more to reserve capacity following brace-gusset weld fracture than to the brace-gusset weld capacities themselves. As observed previously from both large scale testing and static numerical simulations, reserve capacity from chevron CBFs is highly dependent on beam midspan bending following loss of one brace within a story. The OCBF provisions require beams to be designed for an imbalanced force between the tension and compression braces when the braces are in a chevron configuration, which results in significantly deeper beams than an *R* = 3 chevron counterpart, or even an OCBF split-x counterpart. In these simulations, the OCBF chevrons did not experience the undesirable brace-gusset weld fracture in both braces within a story (Figure 2b); instead, the beneficial beam midspan bending mechanism persisted after brace-gusset weld fracture within a single brace (Figure 2a). This behavior was influenced by several uniform assumptions (connection angle thicknesses, gusset plate dimensions, and effects of beam depth) across the four building models, which slightly under-predicted the demands on the remaining brace within a weakened OCBF chevron bay. Further investigations are ongoing with more accurate portrayals of the deeper beams, gusset plate dimensions, and angle thicknesses specific to OCBF chevrons.

The beam midspan bending phenomenon was observed both in large-scale testing of an *R* = 3 chevron CBF and in static numerical simulations. This beneficial behavior is limited when the braces are in a split-x configuration, as three braces in the "X" will restrain beam-bending at midspan until an additional brace-gusset weld fracture occurs. Although beam midspan bending can develop within a split-x configuration, its effectiveness is minimized because it cannot develop unless significant damage has occurred (i.e. loss of two or more braces within an "X").

Both the large scale tests and static numerical simulations revealed that CBFs using a chevron configuration had a larger ceiling with respect to reserve capacity and collapse prevention when compared to a split-x configuration, and this observation is made again in these dynamic analyses as the R = 3 and OCBF chevrons consistently outperformed their split-x counterparts.

The four buildings exhibited relatively similar drifts under the unscaled (SF = 1.0) GMs. The median maximum story drifts for the four buildings are 1.6%, 1.8%, 1.3%, and 1.4% for the R = 3 chevron, R = 3 split-x, OCBF chevron, and OCBF split-x, respectively. The close proximity of these IDA fractile curves under the unscaled GMs suggests that although the frames exhibit widely different levels of collapse prevention, all frames exhibited a comparable level of performance under an MCE-level seismic event. *Weaving*, which is defined as points on an IDA curve where the structure appears to be headed towards collapse, only to display lower drift levels at a higher SF, is especially visible in the 16% fractile curve for the OCBF split-x building. This behavior is to be expected in nonlinear models such as the ones studied, whose behaviors are dependent on variable sequencing of brittle limit states.

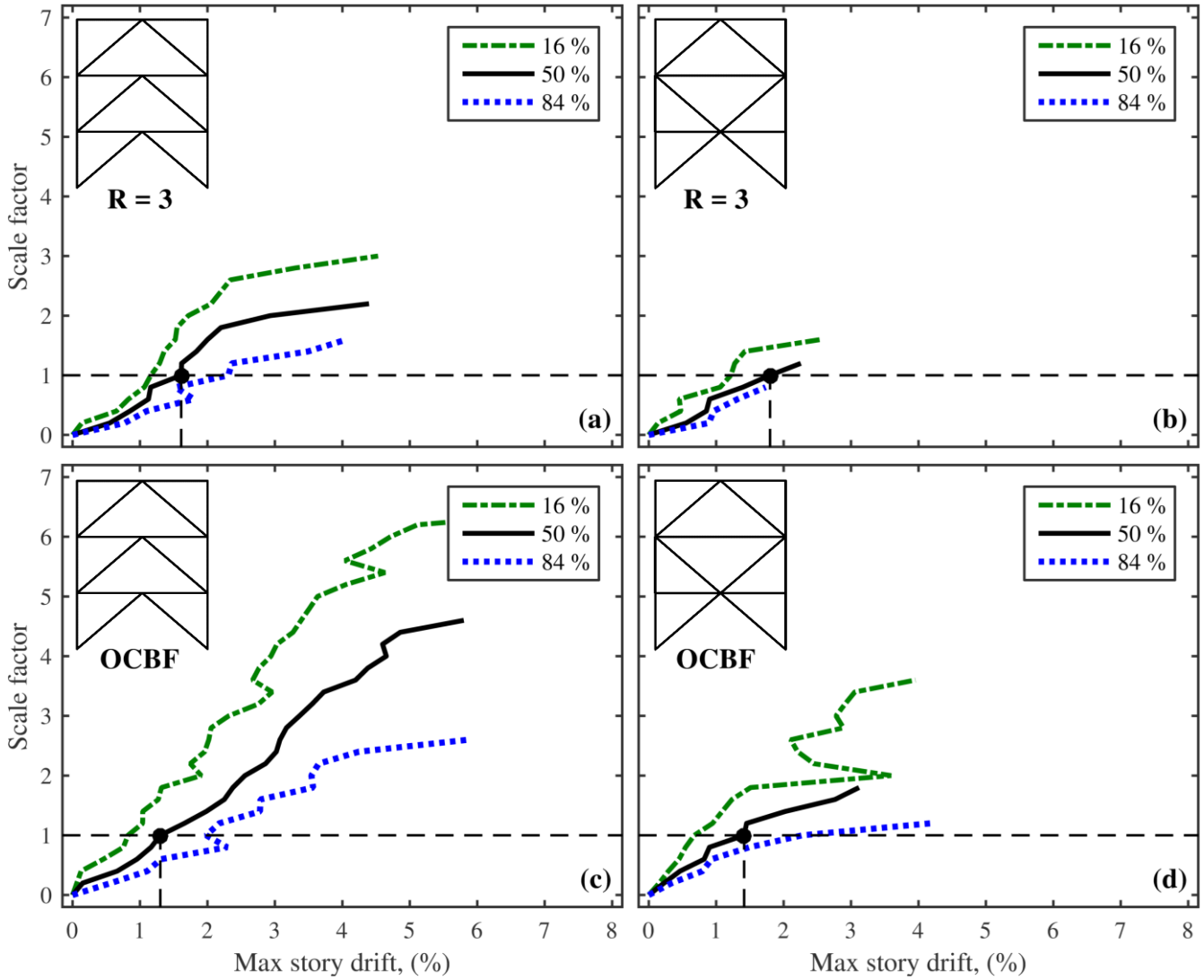

Figure 8 – Multi-record IDA curves for 3-story braced frame buildings designed as: (a) R = 3 chevron; (b) R = 3 split-x; (c) OCBF chevron; and (d) OCBF split-x.

5. Conclusions

The present research has a primary goal of defining and quantifying reserve capacity and its influence on collapse performance in low-ductility CBFs, which are common in moderate seismic regions. Reserve capacity is defined as additional lateral force resisting capacity that is activated after significant damage to the primary SFRS, and may come from a variety of sources within a building, including but not limited to beam-column connections as well as beam and column bending. The project is composed of two primary parts: experimental testing and numerical simulations. To date, experimental tests have been performed on angle components, beam-column connections, and full-scale frames. The full-scale frame tests provided insight into how the selection and interaction of system type (R = 3 or OCBF) and system configuration (chevron or split-x) can influence limit state progression and development of mechanisms, which in turn influence reserve capacity. Numerical frame models were constructed and validated using the experimental tests conducted by the authors to further investigate the influence of system type and system configuration on reserve capacity. A series of static and dynamic numerical simulations were performed on 3-story prototype CBFs in which these parameters (system type and system configuration) were varied.

From the perspective of system configuration, frames using the chevron configuration generally outperformed frames using the split-x configuration. This is due to the beam bending mechanism, which was observed in the static and dynamic chevron frame simulations following loss of a brace within a story. The split-x bracing configuration restricted beam-midspan bending, and these frames were unable to provide comparable reserve capacity. The additional reserve capacity obtained via beam bending contributed to improved collapse performance, as the chevron frames withstood larger drifts and larger GM SFs prior to collapse than their split-x counterparts. From the perspective of system type, the single-record and multi-record dynamic analyses revealed that the OCBFs had better collapse performance than their R = 3 CBF counterparts. In addition to having a larger elastic capacity resulting from increased weld sizes, the OCBFs also exhibited a large reserve capacity due to large member and connection sizes. This was especially noticeable for the OCBF chevron, in which the significantly larger beam sizes contributed to this frame surviving over 50% of GMs with SF = 4.8, compared to the R = 3 chevron in which collapse was prevented under 50% of GMs only up to SF = 2.2.

This study on reserve capacity is ongoing as further numerical simulations are performed on 6- and 9-story braced frames designed using various systems types and system configurations. Additionally, the concept of structural resurrection will be investigated for the frames presented within this paper to give more comprehensive insight into collapse performance. After a baseline performance for R = 3 CBFs and OCBFs is established, steps can be made to present a new design methodology that incorporates reserve capacity through a careful selection of brace orientation, frame geometry, member size, and connection size and type.

6. References

[1] American Society of Civil Engineers (ASCE). (2013). *Minimum Design Loads for Buildings and Other Structures*. ASCE/SEI Standard 7-10. Reston, VA.

[2] American Institute of Steel Construction (AISC). (2010). *Seismic Provisions for Structural Steel Buildings*. AISC 341-10. Chicago, IL.

[3] Tremblay, R., & Stiemer, S. F. (1994). Back-up stiffness for improving the stability of multi-storey braced frames under seismic loading. *Proceedings of the 1994 SSRC Annual Technical Session*, Bethlehem, Pa, 311-325.

[4] Rai, D. C., & Goel, S. C. (2003). Seismic evaluation and upgrading of chevron braced frames. *Journal of Constructional Steel Research*, 59(8), 971-994.

[5] Bruneau, M., Wilson, J.C. and Tremblay, R. (1996) "Performance of steel bridges during the 1995 Hyogo-ken Nanbu (Kobe, Japan) earthquake." *Canadian Journal of Civil Engineering*, 23(3): 678-713.

[6] Clifton, Charles, et al. "Steel Structures Damage from the Christchurch earthquake series of 2010 and 2011." *Bull. New Zealand Society for Earthquake Eng.* 44.4 (2011): 297-318.

[7] Hines, E. M., Appel, M. E., & Cheever, P. J. (2009). Collapse performance of low-ductility chevron braced steel frames in moderate seismic regions. *Engineering Journal*, 46(3), 149.

[8] Sizemore, J., Davaran, A., Fahnestock, L., Tremblay, R., and Hines, E. (2014) Seismic Behavior of Low-Ductility Concentrically-Braced Frames. Structures Congress 2014: pp. 2369-2380. doi: 10.1061/9780784413357.208.

[9] Tremblay, R., Filiatrault, A., Timler, P., & Bruneau, M. (1995). Performance of steel structures during the 1994 Northridge earthquake. *Canadian Journal of Civil Engineering*, 22(2), 338-360.

[10] Liu, J., & Astaneh-Asl, A. (2000). Cyclic testing of simple connections including effects of slab. *Journal of Structural Engineering*, 126(1), 32-39.

[11] Abolmaali, A., Kukreti, A. R., & Razavi, H. (2003). Hysteresis behavior of semi-rigid double web angle steel connections. *Journal of Constructional Steel Research*, 59(8), 1057-1082.

[12] Rai, D. C., & Goel, S. C. (2003). Seismic evaluation and upgrading of chevron braced frames. *Journal of Constructional Steel Research*, 59(8), 971-994.

[13] Beland, T., Bradley, C., Nelson, J., Davaran, A., Hines, E. M., Tremblay, R. & Fahnestock, L. A. (2014). Full-scale testing of beam-column connections with angles. In Proceedings of the 2014 Structures Congress. Boston, MA.

[14] Nelson, J., Bradley, C., Davaran, A., Beland, T., Hines, E. M., Fahnestock, L. A., & Tremblay, R. (2014). Cyclic experimental behavior of angles and applications for connection design and modeling. In Proceedings of the 2014 Structures Congress. Boston, MA.

[15] Nelson, J. (2014). Lateral system design philosophy within moderate seismic regions: Tozzer library case study and angle connection component test program. M.S. Thesis, Tufts University, Medford, MA.

[16] Tremblay, R., Filiatrault, A., Bruneau, M., Nakashima, M., Prion, H. G., & DeVall, R. (1996). Seismic design of steel buildings: lessons from the 1995 Hyogo-ken Nanbu earthquake. *Canadian Journal of Civil Engineering*, 23(3), 727-756.

[17] Stoakes, C. D., & Fahnestock, L. A. (2010). Cyclic flexural testing of concentrically braced frame beam-column connections. *Journal of Structural Engineering*, 137(7), 739-74

[18] Stoakes, C. D., & Fahnestock, L. A. (2012). Cyclic flexural analysis and behavior of beam-column connections with gusset plates. *Journal of Constructional Steel Research*, 72, 227-239.

[19] Bradley, C. (2016). "Experimental investigation of post-elastic failure mechanisms in low-ductility braced frames and the implications for collapse performance." M.S. thesis, Tufts University, Medford, MA.

[20] Sizemore, J.G., Fahnestock, L.A., Hines, E.M. and Bradley, C.R. "Full-Scale Testing of a Low-Ductility Concentrically-Braced Frame," Proceedings, 8th Conf. on Behavior of Steel Structures in Seismic Areas, Shanghai, China, July 2015.

[21] Davaran, A., Beland, T., Fahnestock, L. A., Hines, E. M., & Tremblay, R. (2014). Experimental behavior of low-ductility brace connection limit states. Proceedings, 2014 Struct. Cong.

[22] Shen, J. and A. Astaneh-Asl (1999). "Hysteretic behavior of bolted-angle connections." *Journal of Constructional Steel Research*, 51(3): 201-218.

[23] Garlock, M. M., J. M. Ricles and R. Sause (2003). "Cyclic Load Tests and Analysis of Bolted Top-and-Seat Angle Connections." *Journal of Structural Engineering*, 129(12): 1615-1625.

[24] American Society of Civil Engineers. (2005). Minimum design loads for buildings and other structures. (ASCE 7-05). Reston, VA: American Society of Civil Engineers.

[25] McKenna, F. (1997). "Object oriented finite element programming frameworks for analysis, algorithms and parallel computing." Ph.D. dissertation, Univ. of Calif. at Berkeley, CA.

[26] Karamanci, E., & Lignos, D. G. (2014). Computational approach for collapse assessment of concentrically braced frames in seismic regions. *Journal of Structural Engineering*, 140(8), A4014019.

[27] Hsiao, P. C., Lehman, D. E., & Roeder, C. W. (2012). Improved analytical model for special concentrically braced frames. *Journal of Constructional Steel Research*, 73, 80-94.

[28] Bradley, C., Fahnestock, L., Hines, E., and Sizemore, J. "Full-Scale Cyclic Testing of an Ordinary Concentrically-Braced Frame," ASCE Structures Congress 2015: pp. 702-713. Portland, OR. dx.doi.org/10.1061/9780784479117.061

[29] Sizemore, J. G., Fahnestock, L. A., Hines, E. M., & Bradley, C. R. (2016, submitted). Cyclic analysis of low-ductility concentrically-braced frames. *Journal of Structural Engineering.*

[30] Vamvatsikos D, Cornell CA (2002): Incremental dynamic analysis. *Earthquake Eng. Struct. Dynamics*, 31 (3), 491-514.